Turbulent Flows

Stephen B. Pope
Cambridge University Press, 2000

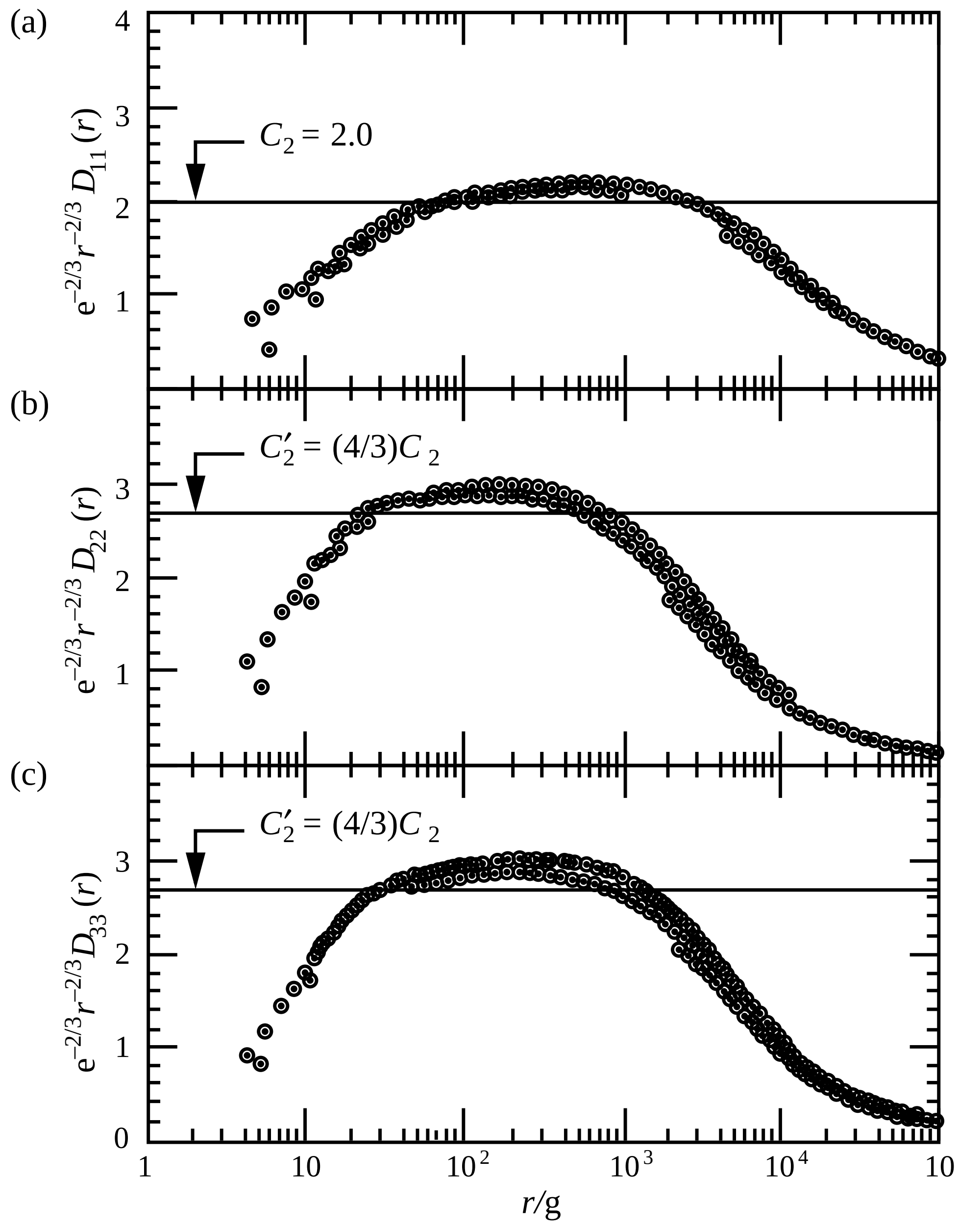

Figure 6.5: Second-order velocity structure functions measured in a high-Reynolds-number turbulent boundary layer. The horizontal lines show the predictions of the Kolmogorov hypotheses in the inertial subrange, Eqs. (6.33) and (6.34). (From Saddoughi and Veeravalli (1994).)

Turbulent Flows

Stephen B. Pope
Cambridge University Press, 2000

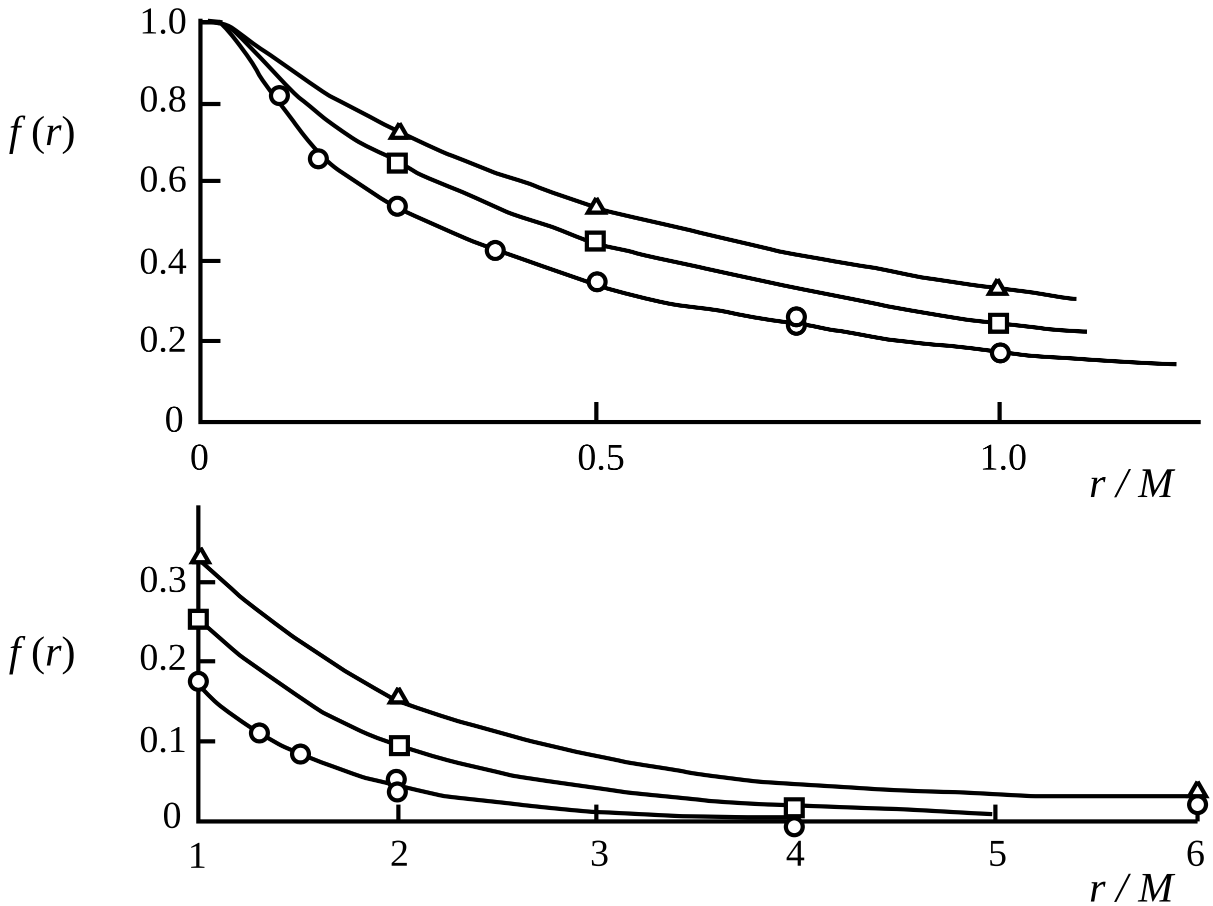

Figure 6.6: Measurements of the longitudinal velocity autocorrelation functions $f(r,t)$ in grid turbulence: $x_1/M = 42, \circ; 98, \Box; 172, \triangle$. (From Comte-Bellot and Corsin (1971).)

Turbulent Flows

Stephen B. Pope
Cambridge University Press, 2000

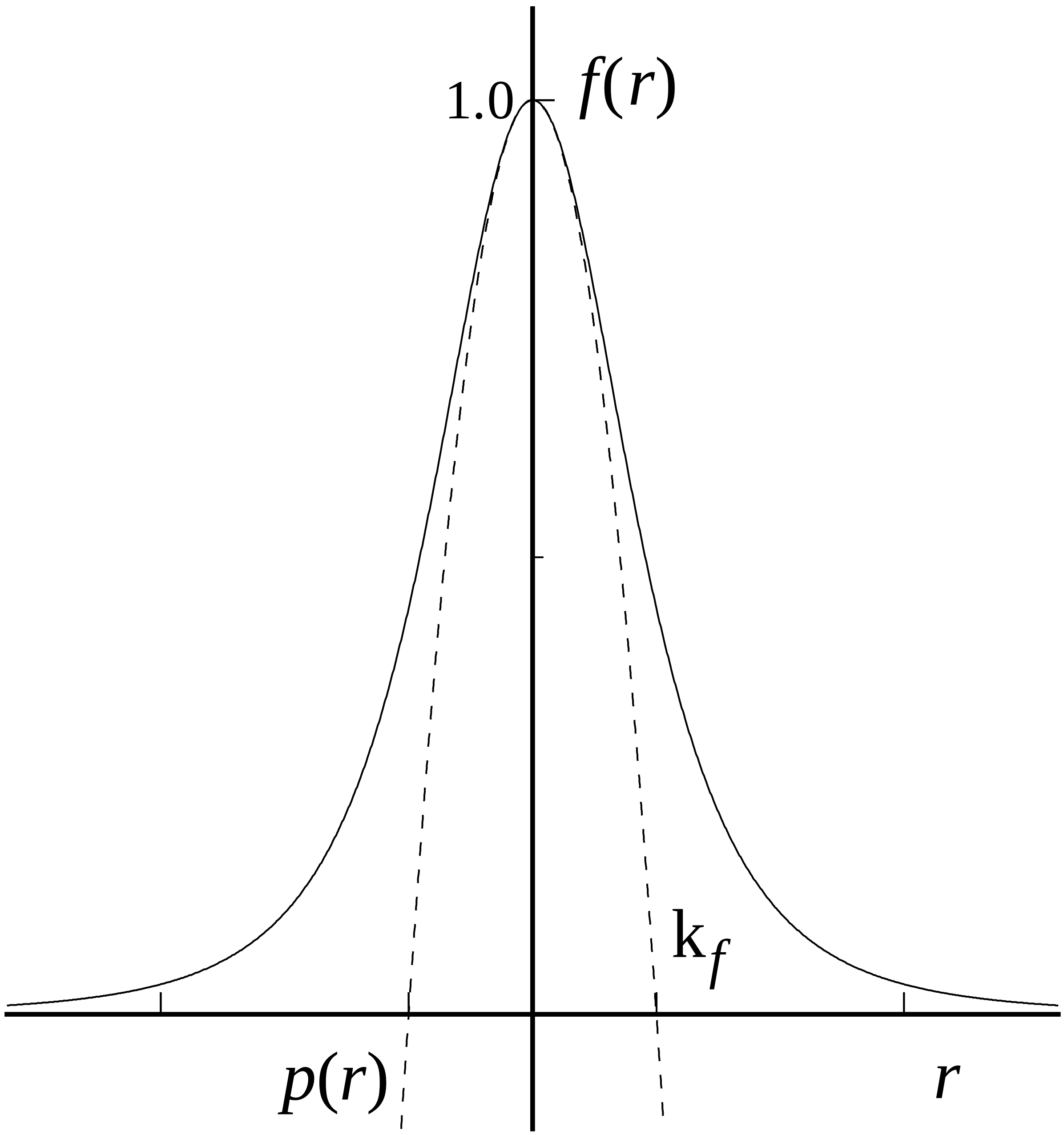

Figure 6.7: Sketch of the longitudinal velocity autocorrelation function showing the definition of the Taylor microscale λ_f.

Turbulent Flows

Stephen B. Pope
Cambridge University Press, 2000

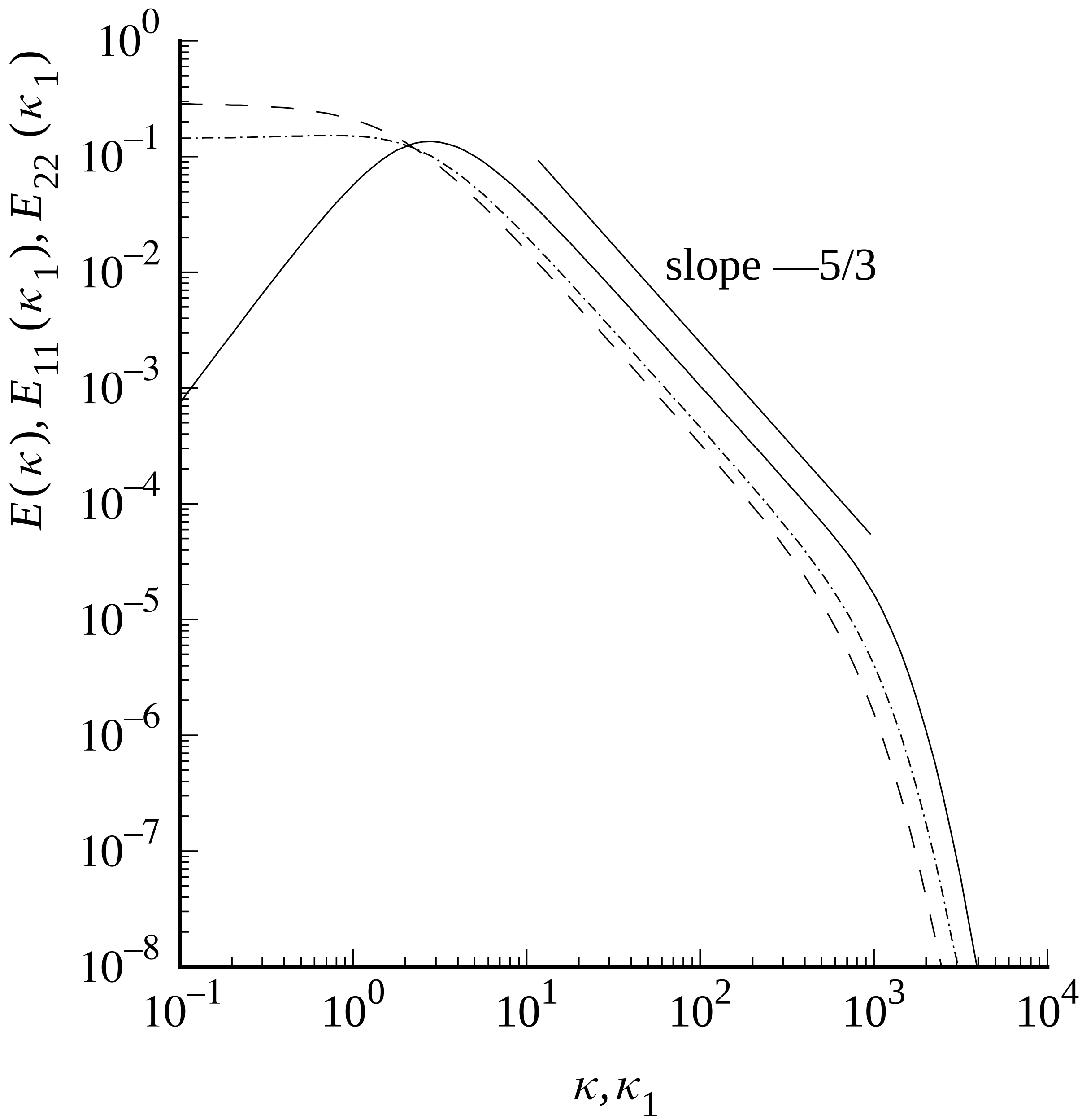

Figure 6.11: Comparison of spectra in isotropic turbulence at $R_\lambda = 500$: solid line, $E(\kappa)$; dashed line, $E_{11}(\kappa_1)$; dot-dashed line, $E_{22}(\kappa_1)$. From the model spectrum, Eq. (6.246). (Arbitrary units.)

Turbulent Flows

Stephen B. Pope
Cambridge University Press, 2000

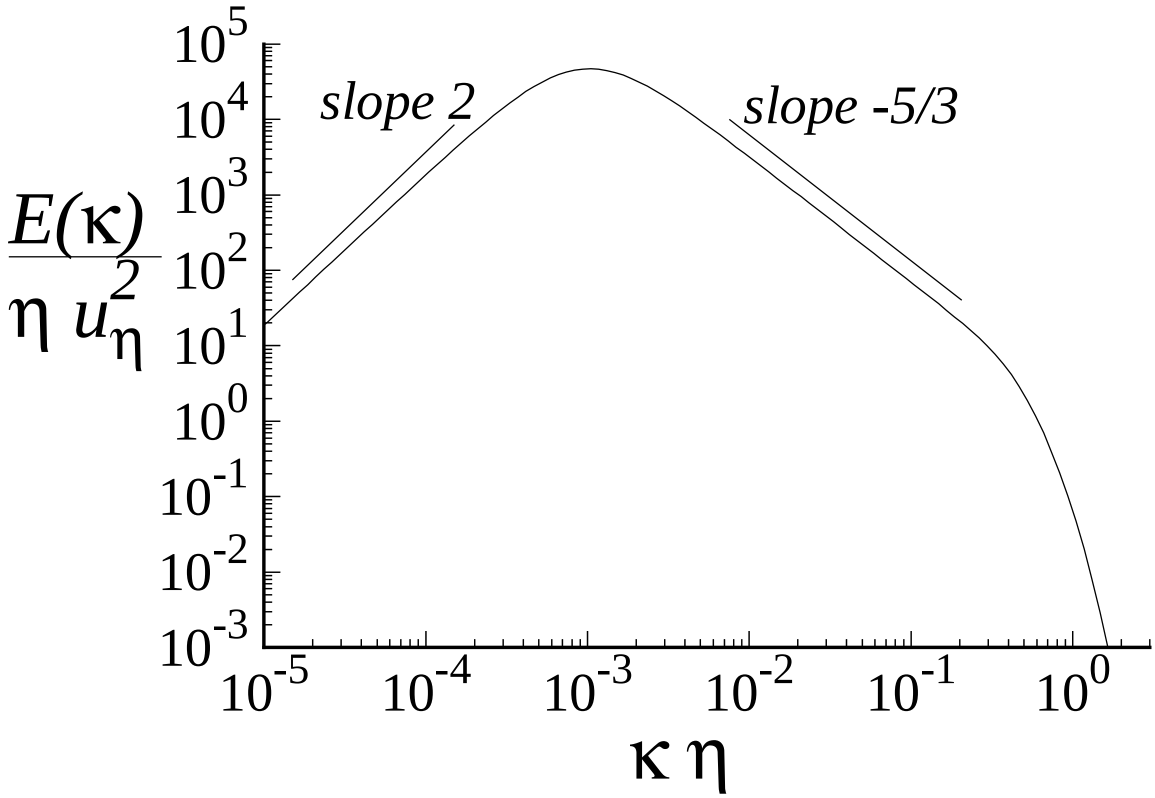

Figure 6.13: Model spectrum (Eq. 2.246) for $R_\lambda = 500$ normalized by the Kolmogorov scales.

Turbulent Flows

Stephen B. Pope
Cambridge University Press, 2000

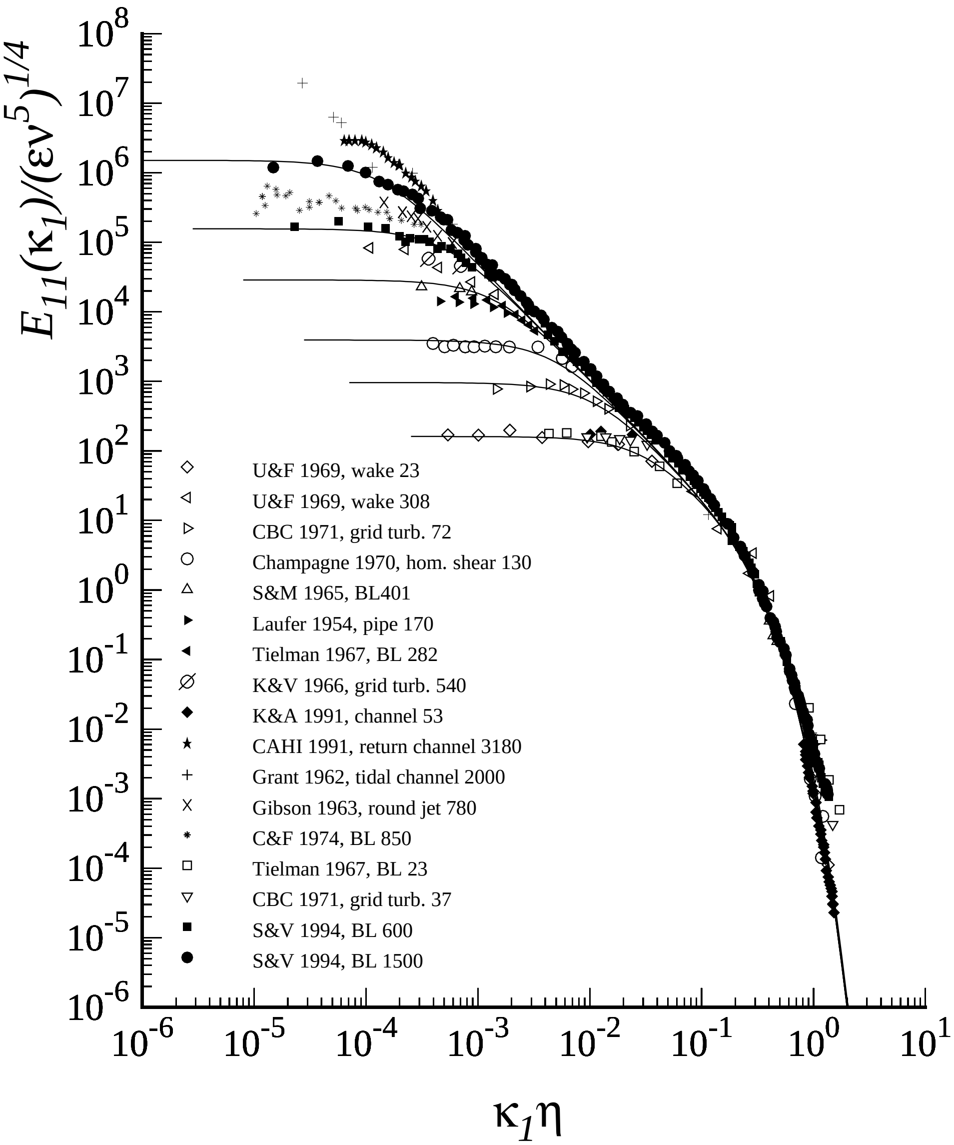

Figure 6.14: Measurements of one-dimensional longitudinal velocity spectra (symbols), and model spectra (Eq. 6.246) for $R_\lambda = 30, 70, 130, 300, 600$ and 1500 (lines). The experimental data are taken from Saddoughi and Veeravalli (1994) where references to the different experiments are given. For each experiment, the final number in the key is the value of R_λ.

Turbulent Flows

Stephen B. Pope

Cambridge University Press, 2000

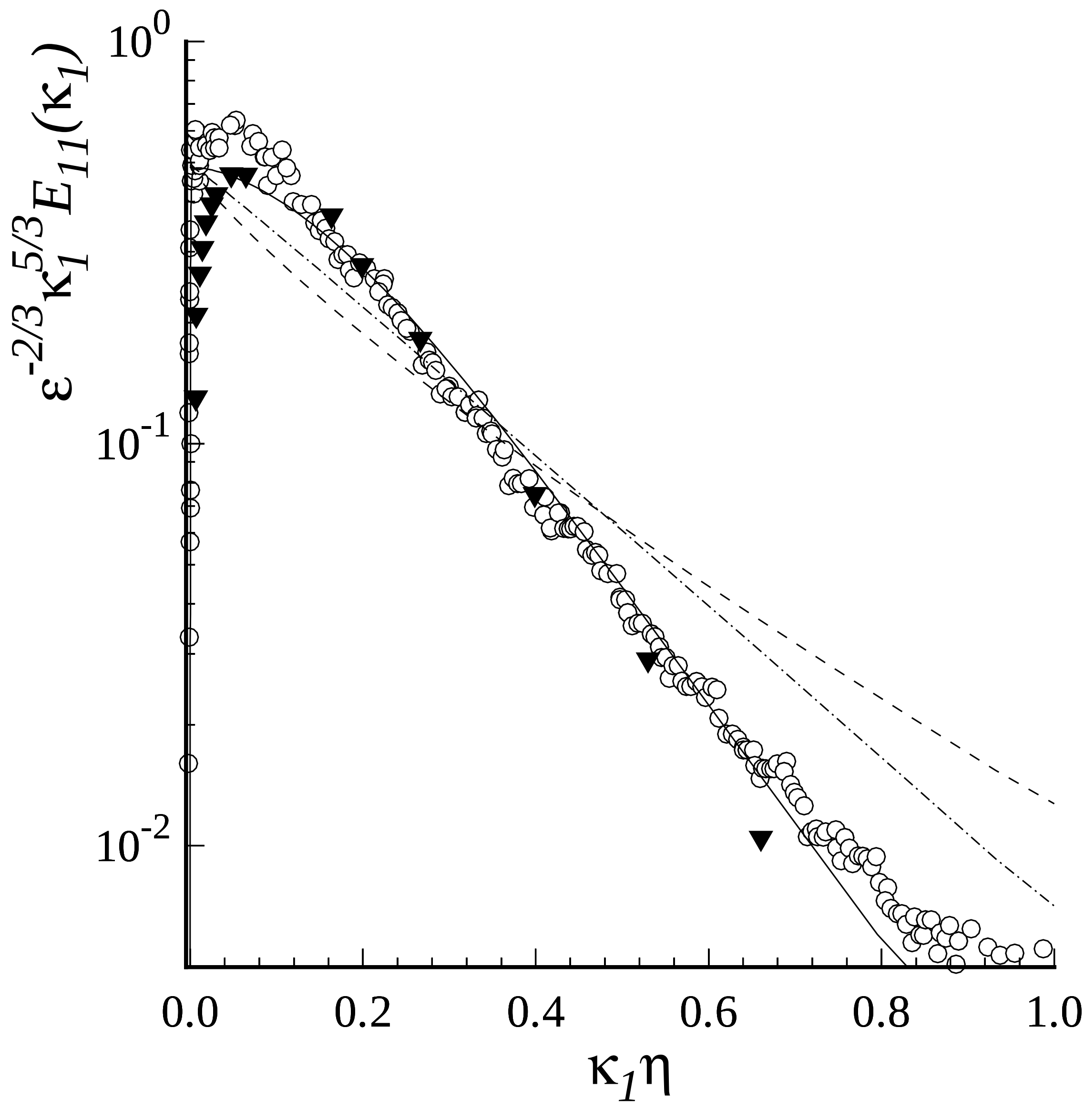

Figure 6.15: Compensated one-dimensional velocity spectra. Measurements of Comte-Bellot and Corrsin (1971) in grid turbulence at $R_\lambda \approx 60$ (triangles), and of Saddoughi and Veeravalli (1994) in a turbulent boundary layer at $R_\lambda \approx 600$ (circles). Solid line, model spectrum Eq. (6.246) for $R_\lambda = 600$; dashed line, exponential spectrum Eq. (6.253); dot-dashed line, Pao's spectrum Eq. (6.254).

Turbulent Flows

Stephen B. Pope

Cambridge University Press, 2000

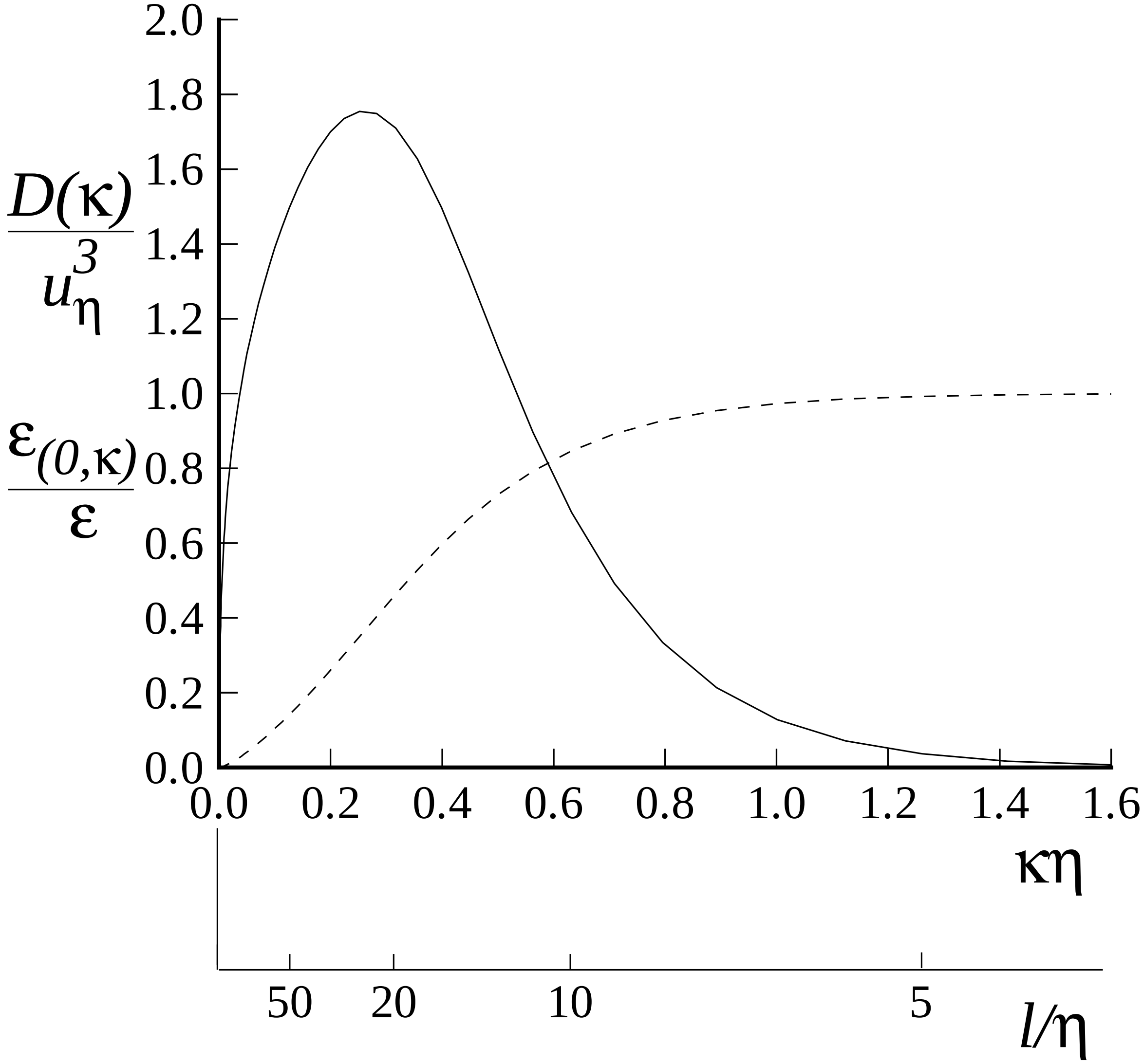

Figure 6.16: Dissipation spectrum (solid line) and cumulative dissipation (dashed line) corresponding to the model spectrum Eq. (6.246) for $R_\lambda = 600$: $\ell = 2\pi/\kappa$ is the wavelength corresponding to wavenumber κ.

Turbulent Flows

Stephen B. Pope
Cambridge University Press, 2000

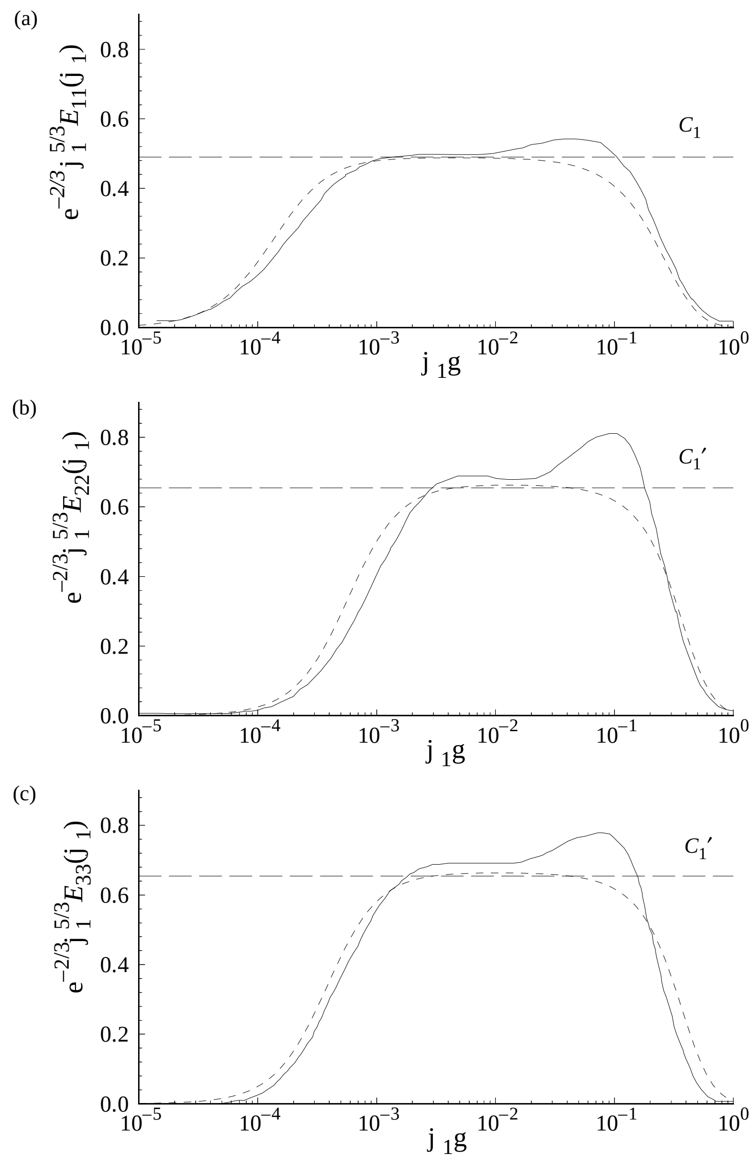

Figure 6.17: Compensated one-dimensional spectra measured in a turbulent boundary layer at $R_\lambda \approx 1,450$. Solid lines, experimental data Saddoughi and Veeravalli (1994); dashed lines, model spectra from Eq. (6.246); long dashed lines, C_1 and C_1' corresponding to Kolmogorov inertial-range spectra. (For E_{11}, E_{22} and E_{33} the model spectra are for $R_\lambda = 1,450$, 690 and 910, respectively, corresponding to the measured values of $\langle u_1^2 \rangle$, $\langle u_2^2 \rangle$ and $\langle u_3^2 \rangle$.)

Turbulent Flows

Stephen B. Pope
Cambridge University Press, 2000

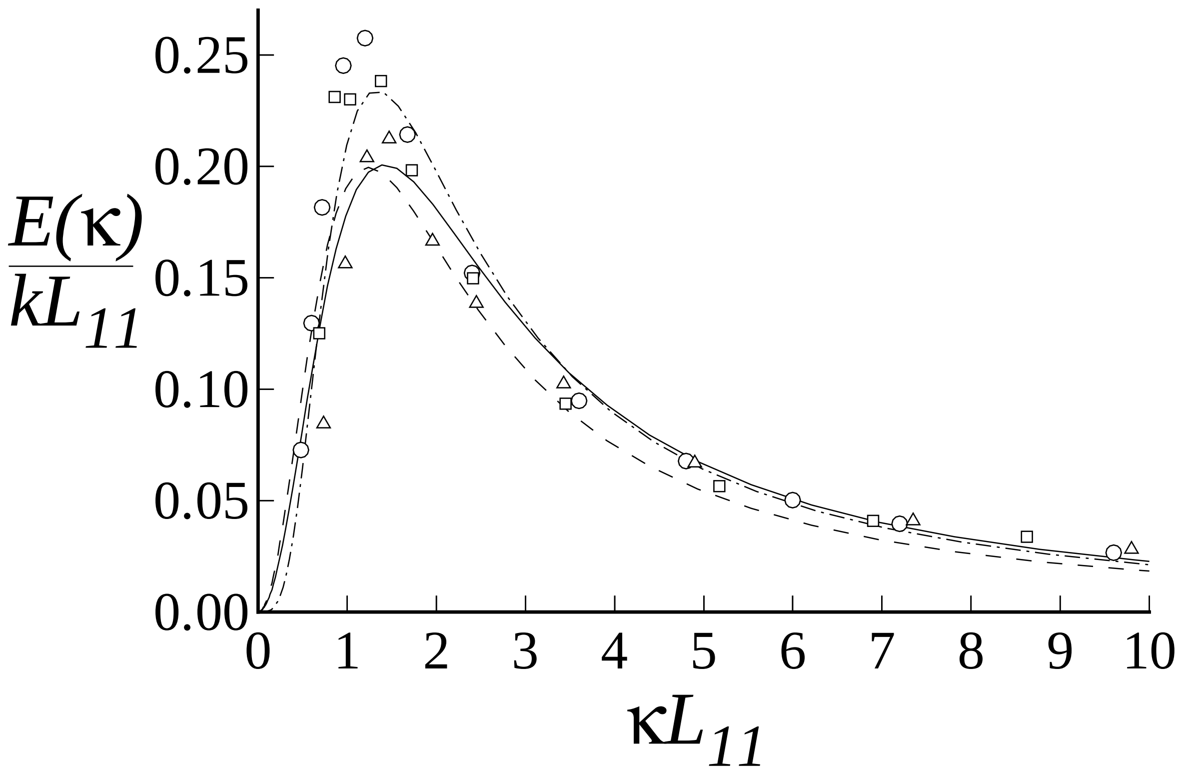

Figure 6.18: Energy spectrum function in isotropic turbulence normalized by k and L_{11}. Symbols, grid-turbulence experiments of Comte-Bellot and Corrsin (1971): $\bigcirc, \mathrm{R}_\lambda = 71$; $\square, \mathrm{R}_\lambda = 65$; $\triangle, \mathrm{R}_\lambda = 61$. Lines, model spectrum, Eq. (6.246): solid, $p_0 = 2$, $\mathrm{R}_\lambda = 60$; dashed, $p_0 = 2$, $\mathrm{R}_\lambda = 1,000$; dot-dash $p_0 = 4$, $\mathrm{R}_\lambda = 60$.

Turbulent Flows

Stephen B. Pope
Cambridge University Press, 2000

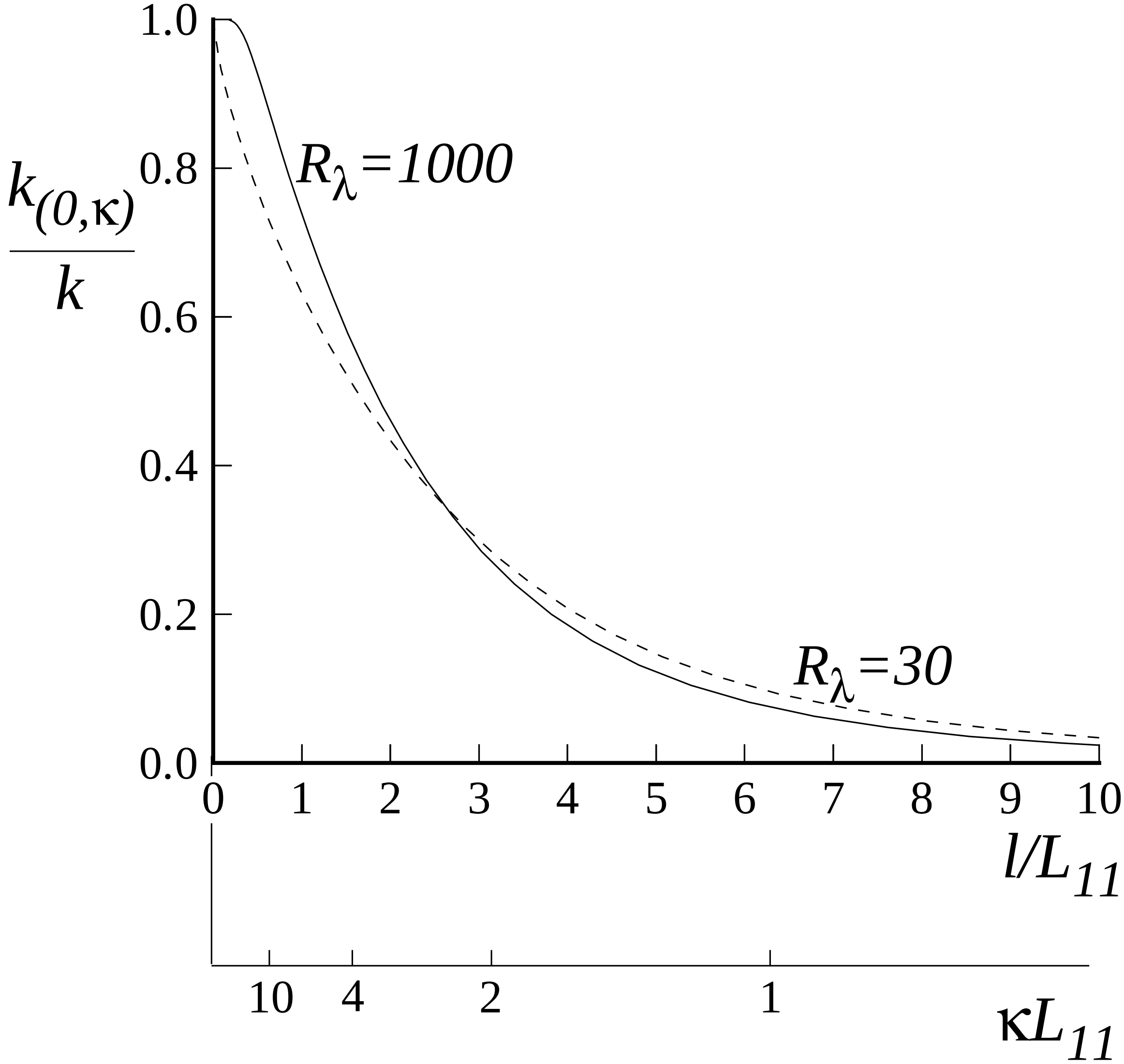

Figure 6.19: Cumulative turbulent kinetic energy $k_{(0,\kappa)}$ against wavenumber κ and wavelength $\ell = 2\pi/\kappa$ for the model spectrum.

Turbulent Flows

Stephen B. Pope
Cambridge University Press, 2000

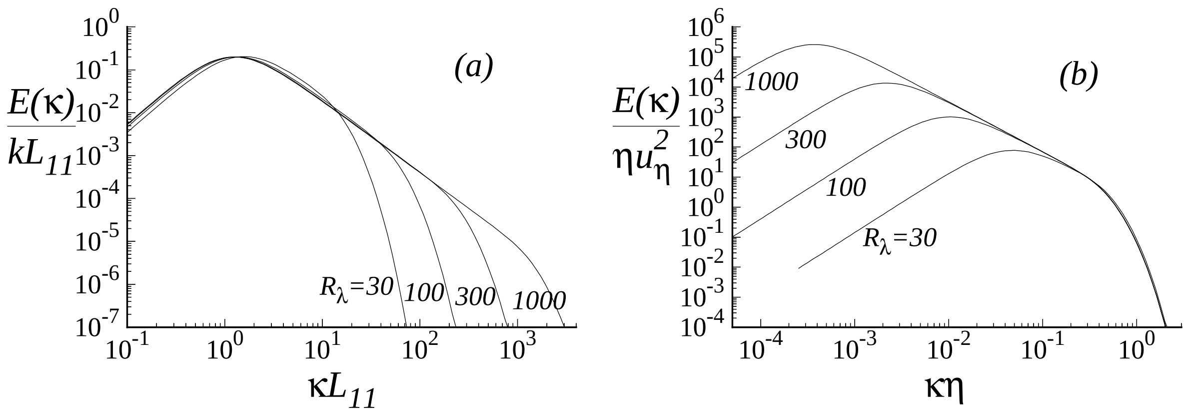

Figure 6.20: Model spectrum for different Reynolds numbers, scaled by (a) k and L_{11} (b) Kolmogorov scales.

Turbulent Flows

Stephen B. Pope
Cambridge University Press, 2000

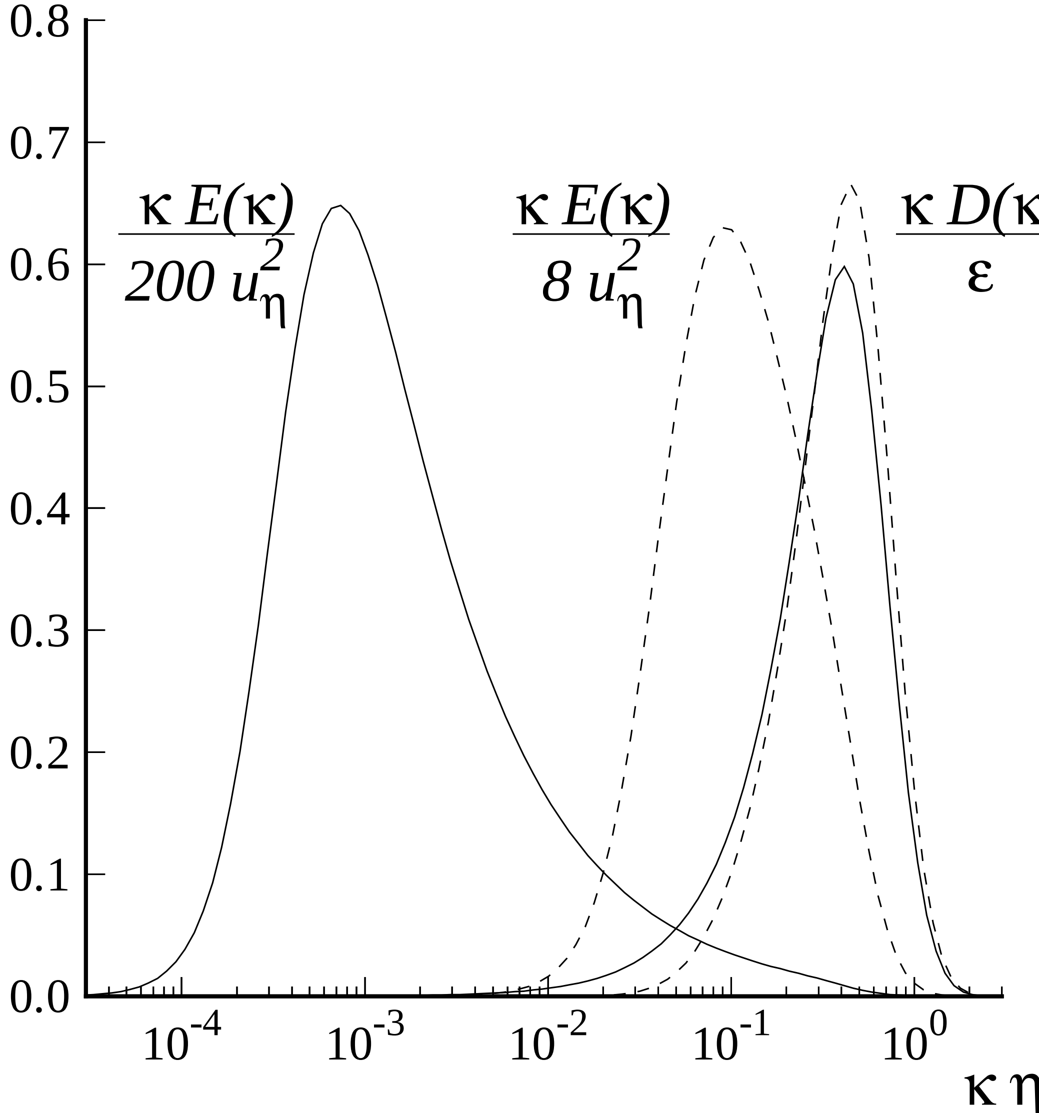

Figure 6.21: Model energy and dissipation spectra normalized by the Kolmogorov scales at $R_\lambda = 1,000$ (solid lines) and $R_\lambda = 30$ (dashed lines). (Note the scaling of $E(\kappa)$.)

Turbulent Flows

Stephen B. Pope

Cambridge University Press, 2000

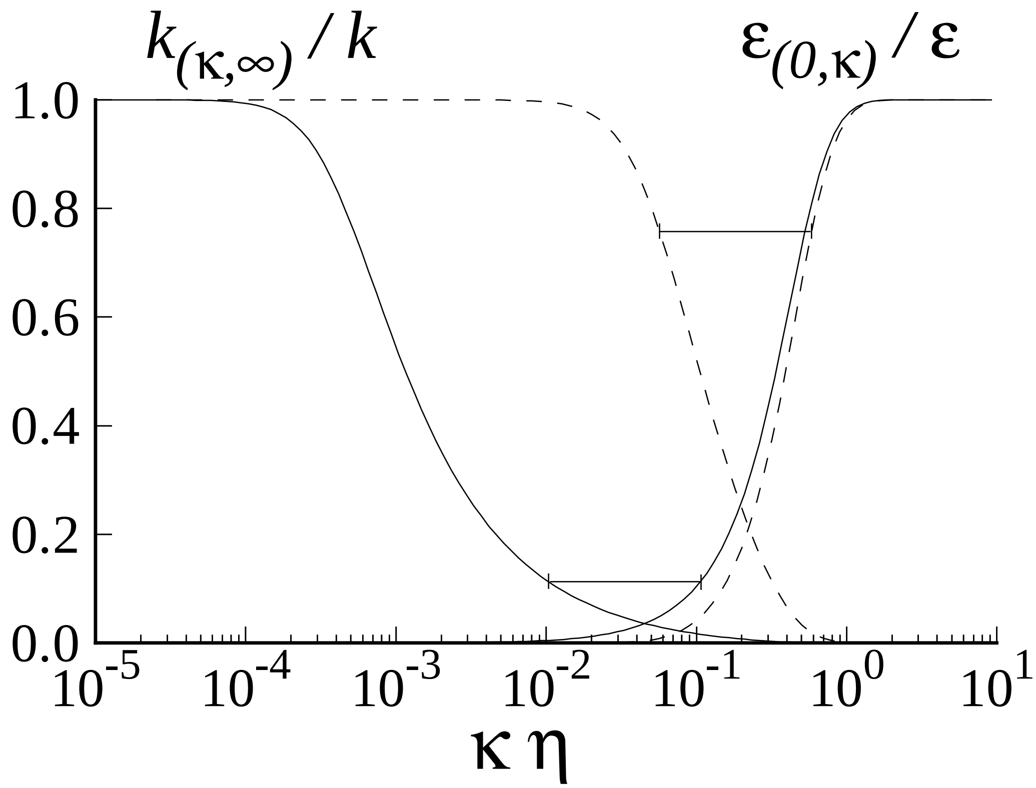

Figure 6.22: The fraction of the energy at wavenumbers greater than κ $(k_{(\kappa,\infty)}/k)$ and the fraction of the dissipation at wavenumbers less than κ $(\varepsilon_{(0,\kappa)}/\varepsilon)$ for the model spectrum at $\mathrm{R}_\lambda = 1,000$ (solid line) and at $\mathrm{R}_\lambda = 30$ (dashed line). For the two Reynolds numbers, the horizontal bars identify the "decade of wavenumbers of most overlap" between the energy and dissipation spectra.

Turbulent Flows

Stephen B. Pope
Cambridge University Press, 2000

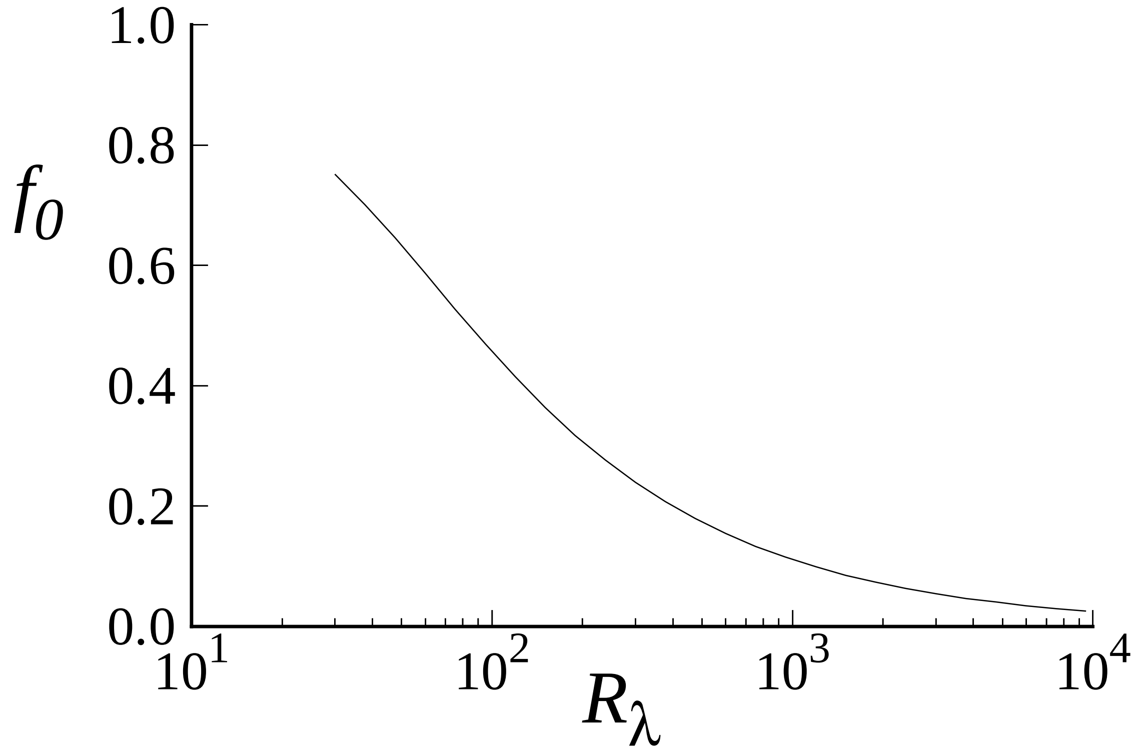

Figure 6.23: Fraction f_0 of the energy and dissipation contributed by the wavenumber decade of maximum overlap as a function of R_λ for the model spectrum.

Turbulent Flows

Stephen B. Pope
Cambridge University Press, 2000

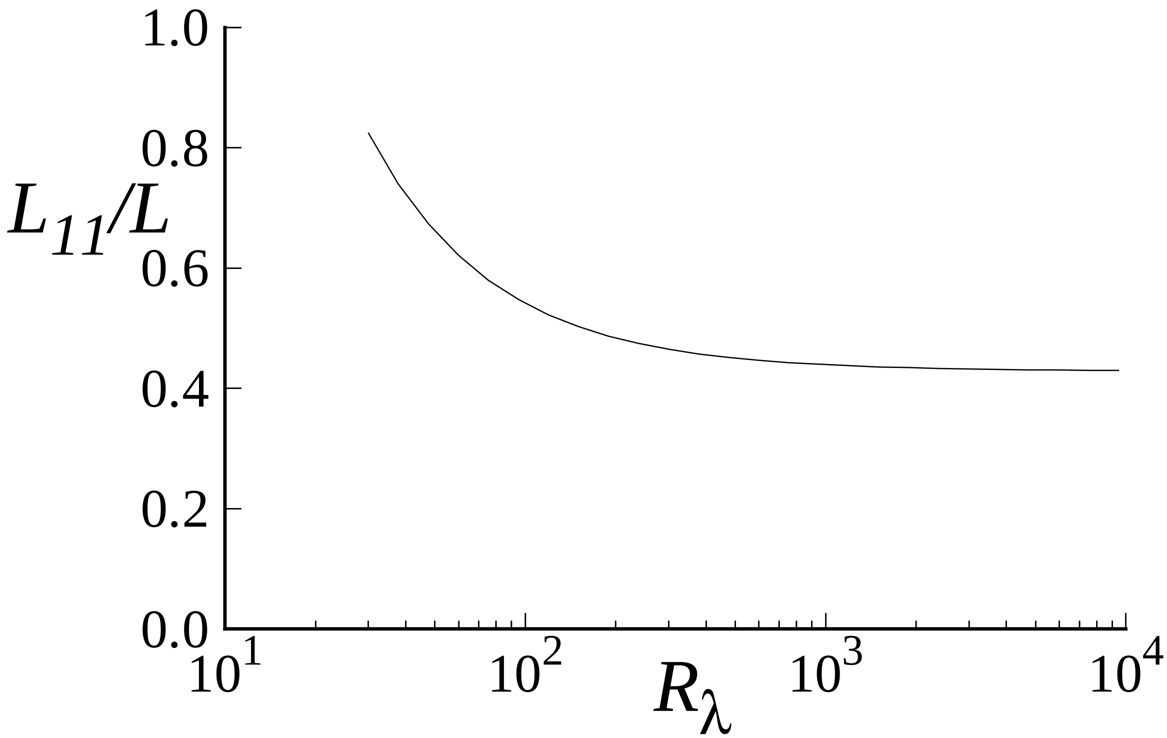

Figure 6.24: Ratio of the longitudinal integral lengthscale L_{11} to $L = k^{\frac{3}{2}}/\varepsilon$ as a function of Reynolds number for the model spectrum.

Turbulent Flows

Stephen B. Pope
Cambridge University Press, 2000

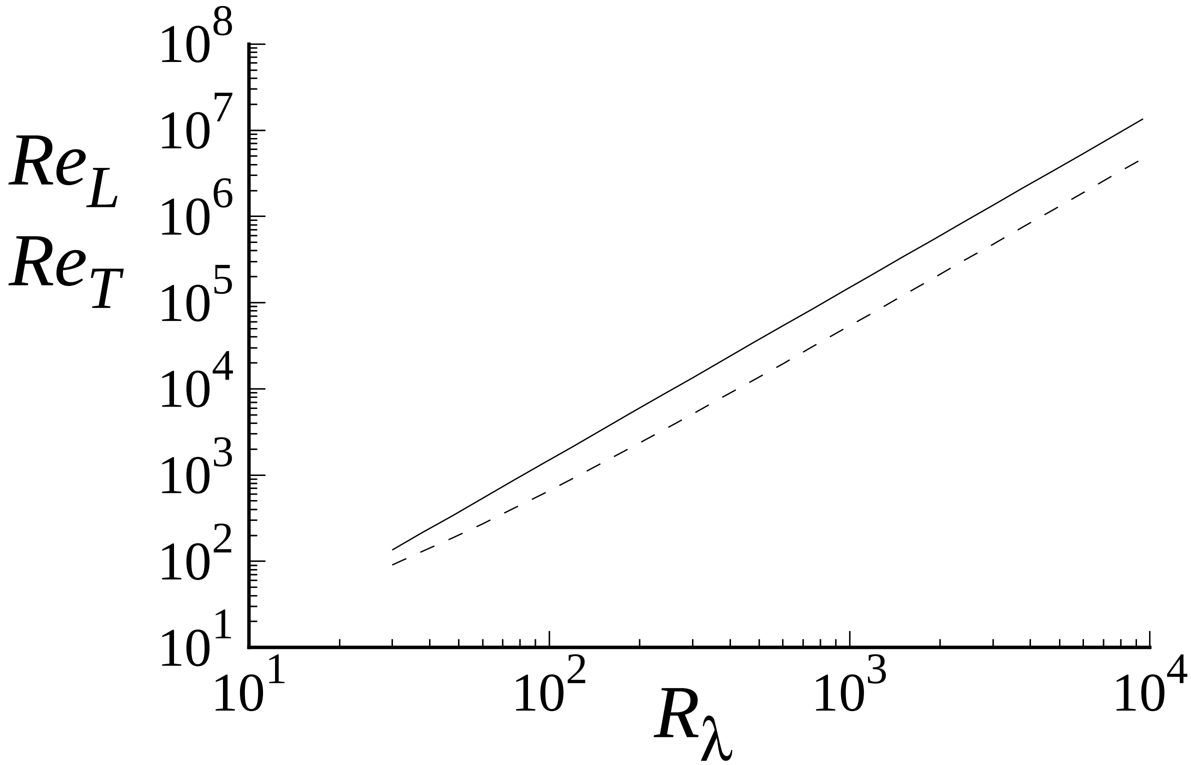

Figure 6.25: Turbulence Reynolds numbers Re_L (solid line) and Re_T (dashed line) as functions of R_λ for the model spectrum.

Turbulent Flows

Stephen B. Pope
Cambridge University Press, 2000

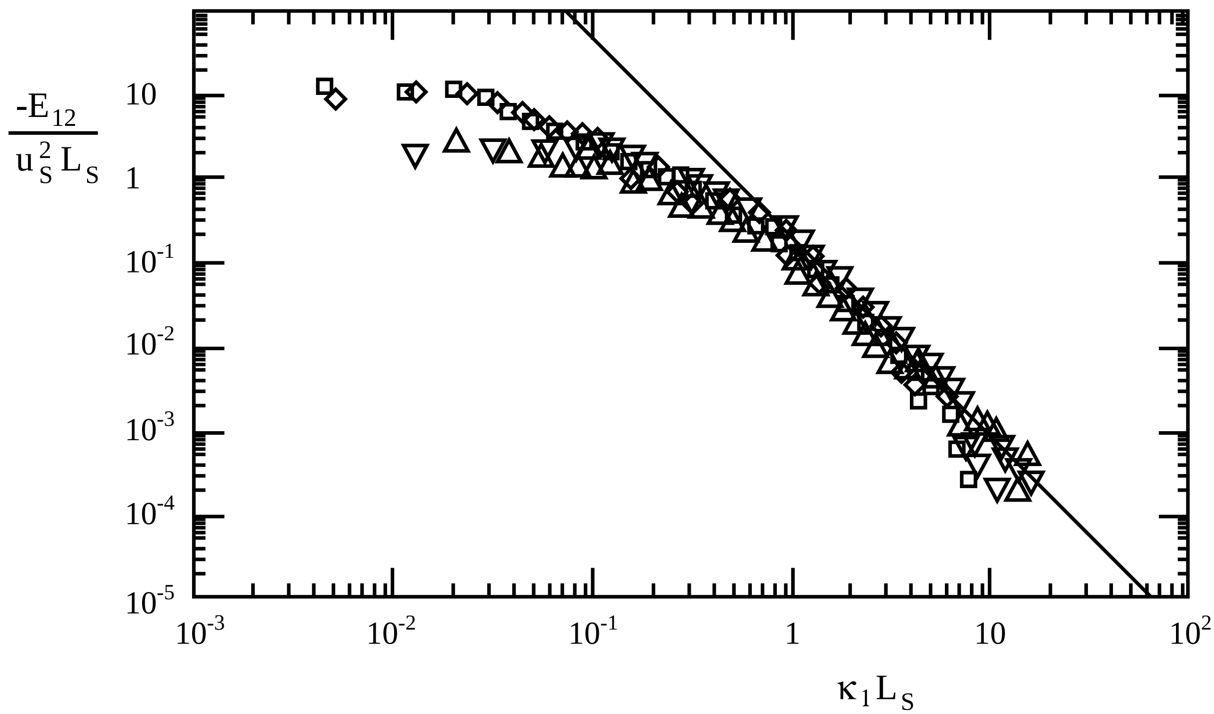

Figure 6.26: Shear-stress spectra scaled by $u_{\mathcal{S}}$ and $L_{\mathcal{S}}$: line, Eq. (6.277) with $C_{12} = 0.15$; symbols, experimental data of Saddoughi and Veeravalli (1994) from turbulent boundary layers with $\mathrm{R}_\lambda \approx 500$ to 1,450.

Turbulent Flows

Stephen B. Pope
Cambridge University Press, 2000

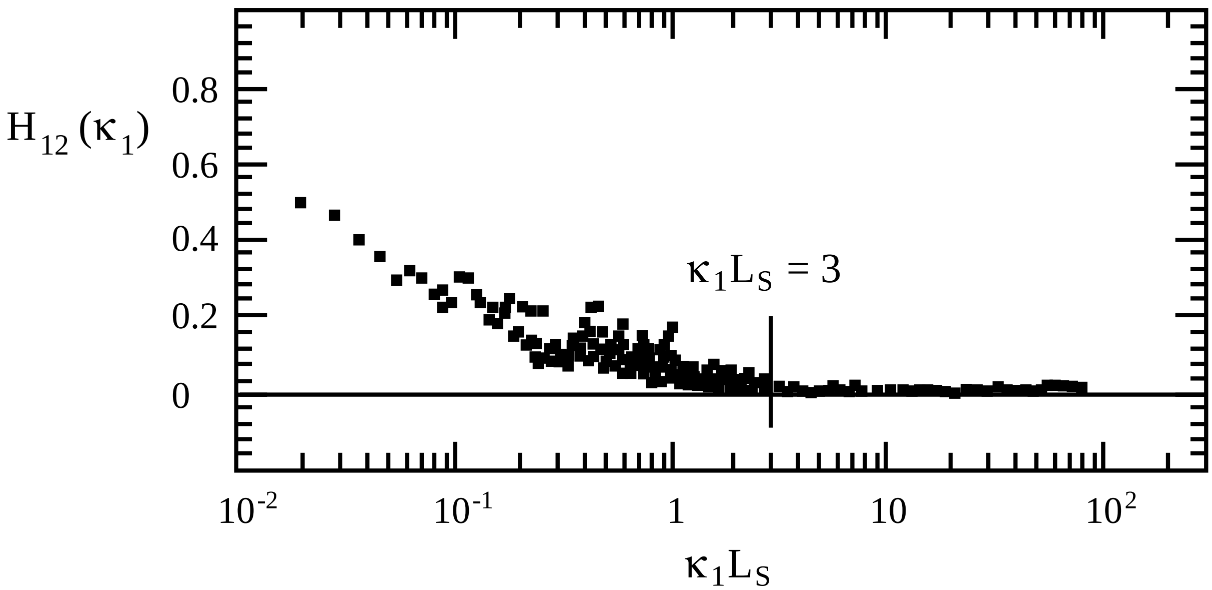

Figure 6.27: Spectral coherency measured in a turbulent boundary layer at $R_\lambda = 1400$ (Saddoughi and Veeravalli 1994).

Turbulent Flows

Stephen B. Pope
Cambridge University Press, 2000

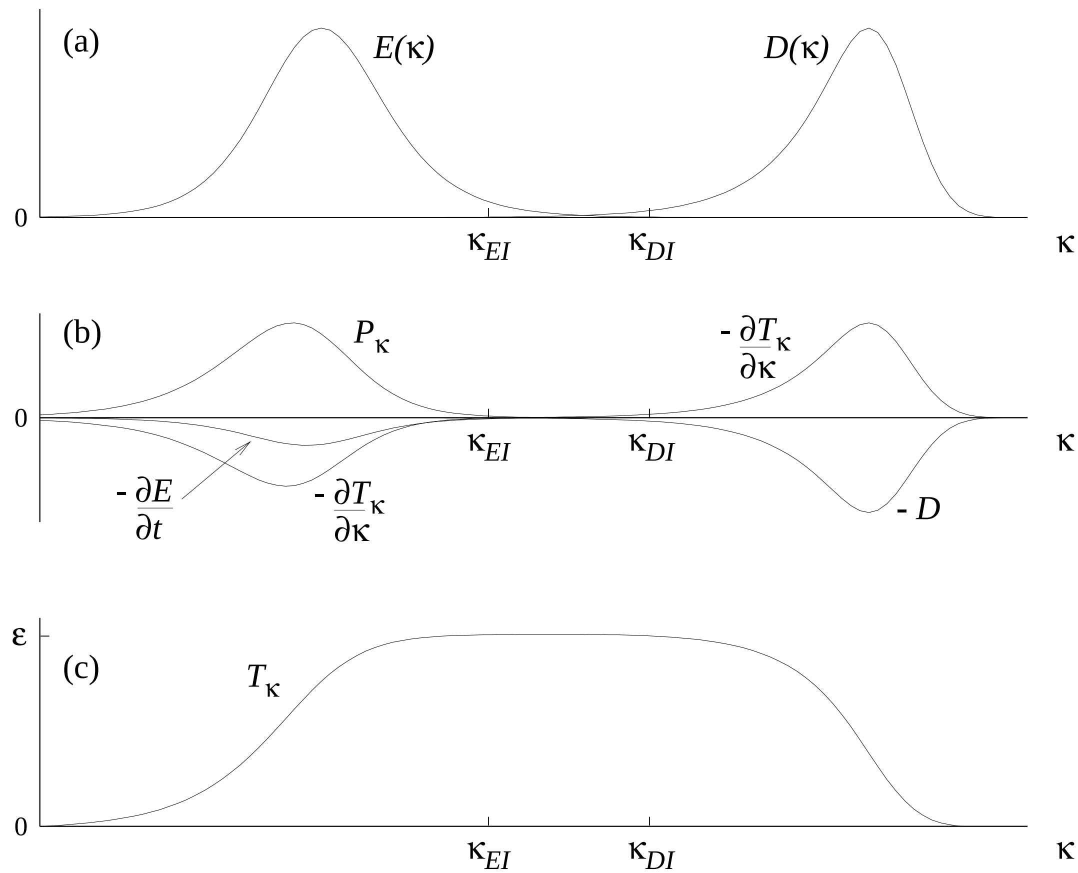

Figure 6.28: For homogeneous turbulence at very high Reynolds number, sketches of (a) the energy and dissipation spectra (b) the contributions to the balance equation for $E(\kappa, t)$ (Eq. 6.284), and (c) the spectral energy transfer rate.

Turbulent Flows

Stephen B. Pope
Cambridge University Press, 2000

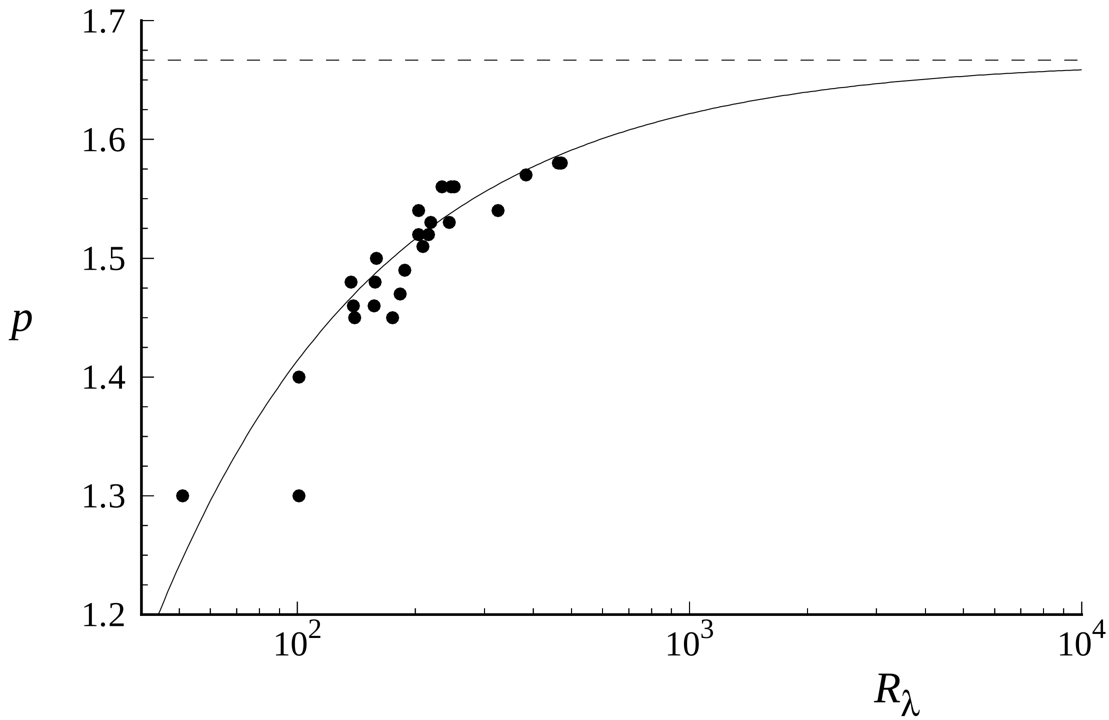

Figure 6.29: Spectrum power-law exponent p ($E(\kappa) \sim \kappa^{-p}$) as a function of Reynolds number in grid turbulence: symbols, experimental data of Mydlarski and Warhaft (1998); dashed line, $p = \frac{5}{3}$; solid line, empirical curve $p = \frac{5}{3} - 8\mathrm{R}_\lambda^{-\frac{3}{4}}$.

Turbulent Flows

Stephen B. Pope
Cambridge University Press, 2000

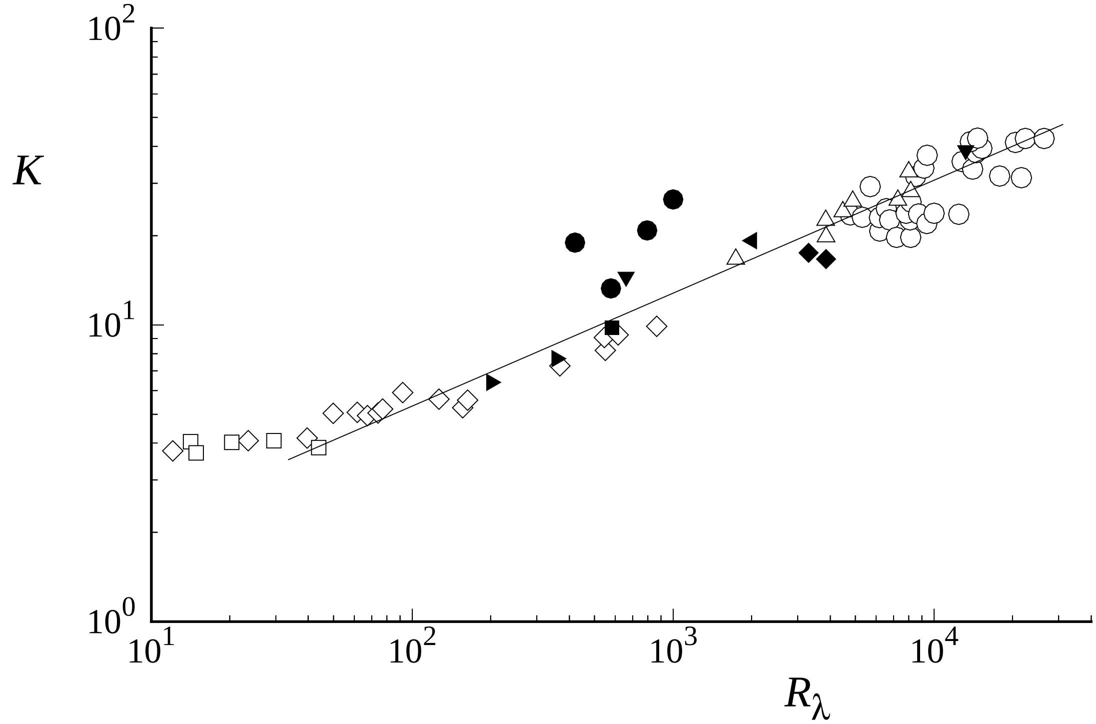

Figure 6.30: Measurements (symbols) compiled by Van Atta and Antonia (1980) of the velocity-derivative kurtosis as a function of Reynolds number. The solid line is $K \sim \mathrm{R}_\lambda^{\frac{3}{8}}$.

Turbulent Flows

Stephen B. Pope
Cambridge University Press, 2000

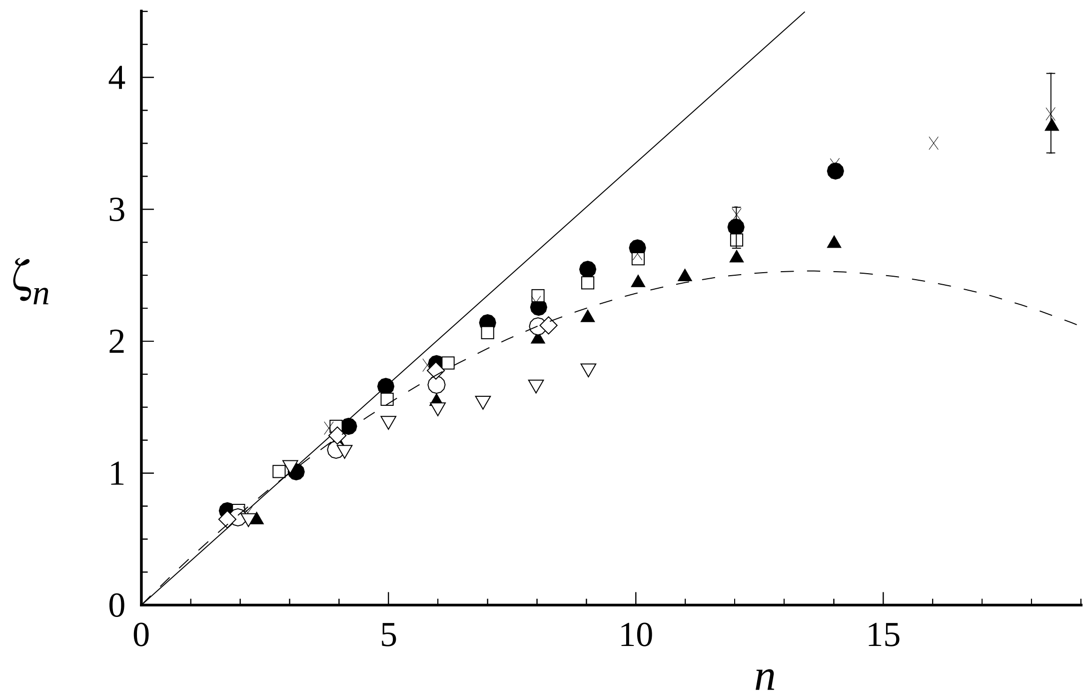

Figure 6.31: Measurements (symbols) compiled by Anselmet *et al.* (1984) of the longitudinal velocity structure function exponent ζ_n in the inertial subrange, $D_n(r) \sim r^{\zeta_n}$. The solid line is the Kolmogorov (1941) prediction, $\zeta_n = \frac{1}{3}n$: the dashed line is the prediction of the refined similarity hypothesis, Eq. (6.323) with $\mu = 0.25$.

Turbulent Flows

Stephen B. Pope
Cambridge University Press, 2000

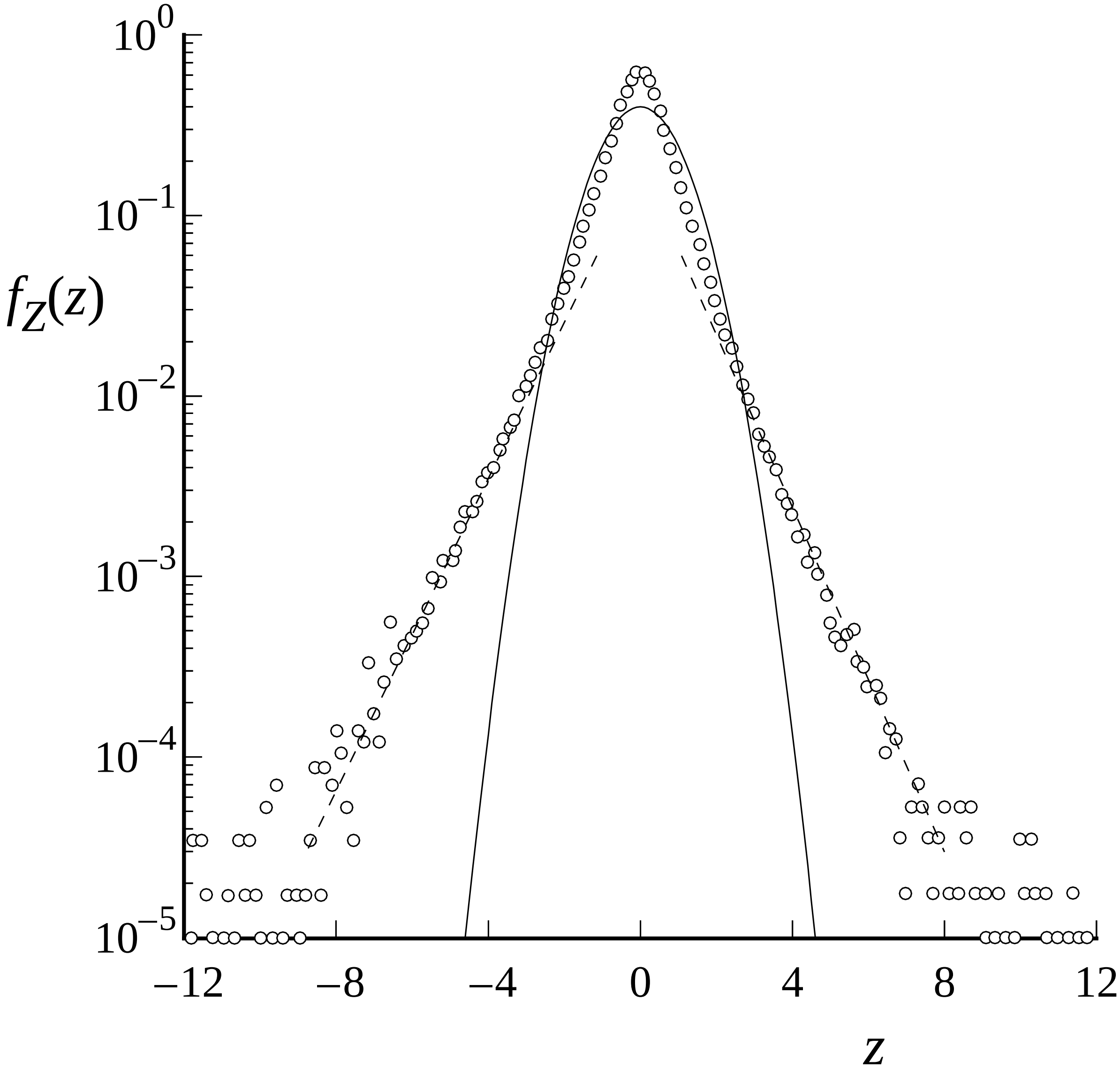

Figure 6.32: PDF $f_Z(z)$ of the normalized velocity derivative $Z \equiv (\partial u_1/\partial x_1)/\langle(\partial u_1/\partial x_1)^2\rangle^{\frac{1}{2}}$ measured by Van Atta and Chen (1970) in the atmospheric boundary layer (high Re). The solid line is a Gaussian; the dashed lines correspond to exponential tails (Eqs. 6.309 and 6.310).

Turbulent Flows

Stephen B. Pope
Cambridge University Press, 2000

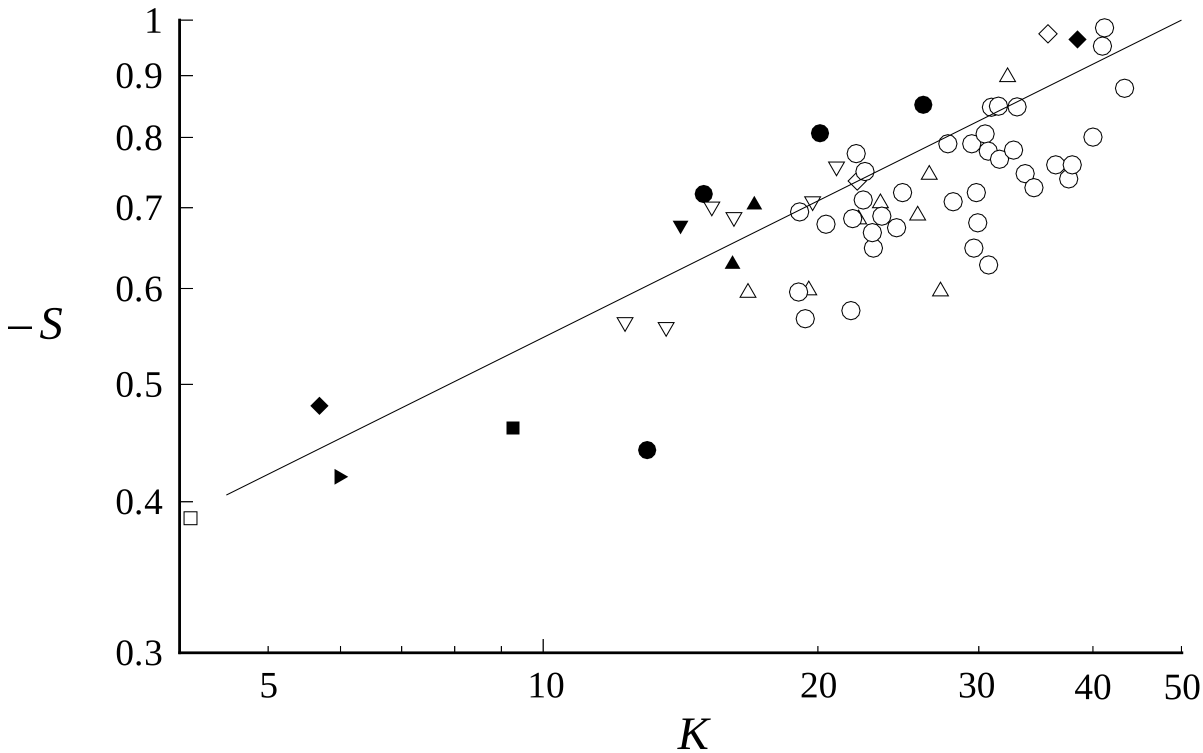

Figure 6.33: Measurements compiled by Van Atta and Antonia (1980) of the velocity-derivative skewness S and kurtosis K. The line is $-S \sim K^{\frac{3}{8}}$.